Research Square

Preprints are preliminary reports that have not undergone peer review.
They should not be considered conclusive, used to inform clinical practice,
or referenced by the media as validated information.

Plasma Channel Characterisation and Particle-in-Cell Modelling of Discharge-Capillary Targets for Laser-Plasma Accelerators.

Alex Whitehead

alex.whitehead@eli-laser.eu

Extreme Light Infrastructure ERIC (Czech Republic)

Mihail Miceski

Extreme Light Infrastructure ERIC (Czech Republic)

Srimanta Maity

Physical Research Laboratory

Martin Matys

Extreme Light Infrastructure ERIC (Czech Republic)

Sebastian Niekrasz

Extreme Light Infrastructure ERIC (Czech Republic)

Petr Zimmermann

Extreme Light Infrastructure ERIC (Czech Republic)

Pavel V. Sasorov

Extreme Light Infrastructure ERIC (Czech Republic)

Alexandr Jančárek

Czech Technical University in Prague

Jonathan T. Green

Extreme Light Infrastructure ERIC (Czech Republic)

Alexander Molodozhentsev

Extreme Light Infrastructure ERIC (Czech Republic)

Research Article

Keywords: Laser-plasma accelerator, Capillary discharge, Laser guiding, Particle-in-cell simulations

Posted Date: September 15th, 2026

DOI: https://doi.org/10.21203/rs.3.rs-10869860/v1

License: This work is licensed under a Creative Commons Attribution 4.0 International License.
Read Full License

Additional Declarations: No competing interests reported.

Plasma Channel Characterisation and Particle-in-Cell Modelling of Discharge-Capillary Targets for Laser-Plasma Accelerators

Alex Whitehead[1,2*], Mihail Miceski[1,2], Srimanta Maity[3], Martin Matys[1], Sebastian Niekrasz[1,4], Petr Zimmermann[1], Pavel V. Sasorov[1], Alexandr Jančárek[1,2], Jonathan T. Green[1], Alexander Molodozhentsev[1]

[1*]The Extreme Light Infrastructure ERIC, ELI Beamlines Facility, Za Radnicí 835, 252 41, Dolní Břežany, Czech Republic.
[2]Czech Technical University in Prague, Faculty of Nuclear Sciences and Physical Engineering, Břehová 7, 110 00, Prague, Czech Republic.
[3]Atomic, Molecular and Optical Physics Division, Physical Research Laboratory, Navrangpura, 380 009, Ahmedabad, India.
[4]Czech Technical University in Prague, Faculty of Electrical Engineering, Technická 2, 166 27, Prague, Czech Republic.

*Corresponding author(s). E-mail(s): alex.whitehead@eli-laser.eu;

Abstract

Laser-plasma accelerators (LPAs) can generate high-energy, high-quality electron beams, paving the way for a new generation of compact free-electron lasers (FELs). To achieve this, beam stability and repeatability must improve, relying on advances in high-power lasers and plasma-source development. These are key technologies for the 100 Hz LPA-based FEL under development at ELI ERIC within the EuPRAXIA project. In this study, we analyse a plasma-target concept designed to generate stable, high-quality electron beams essential for compact extreme-ultraviolet (EUV) FEL applications. We present a gas-filled capillary in which a high-voltage electrical discharge creates a plasma channel. These channels enhance LPA stability by guiding the laser pulse and maintaining its focus, thereby improving energy transfer. The characteristics of the

channel are influenced by the capillary shape, gas conditions, and discharge setup. Furthermore, we investigate the laser–plasma interaction, laser guiding, and electron-beam acceleration using particle-in-cell simulations incorporating the experimentally measured plasma density profile and laser parameters representative of the high-repetition-rate L2-DUHA laser system under development at ELI ERIC.

Keywords: Laser-plasma accelerator, Capillary discharge, Laser guiding, Particle-in-cell simulations

1 Introduction

Plasma-based accelerators (PBAs) have demonstrated the ability to accelerate electrons either by using ultra-intense laser pulses, as in laser wakefield acceleration (LWFA) [1], or by employing charged particle beams to drive plasma waves, as in plasma wakefield acceleration (PWFA) [2].

Recent developments in the PBA community have achieved long-term shot-to-shot stability [3] and high-quality electron beams [4], reaching parameters suitable for free-electron laser (FEL) applications [5–9]. The generation of high-repetition-rate electron beams for various applications remains an important area of current research, particularly with the emergence of 100-TW-class laser systems capable of operating at repetition rates of up to 100 Hz [10]. However, transitioning to high-repetition-rate operation poses dual challenges: laser systems must reliably deliver ultrashort pulses, while target systems require plasma sources capable of sustaining high repetition rates. Developing such high-repetition-rate capabilities is therefore essential for the future 100 Hz LPA-based FEL under development at ELI ERIC [11] within the EuPRAXIA project [12].

In this work, we present our research on the development of a plasma source capable of high-repetition-rate operation for LWFA. We propose the use of a gas-filled capillary in which the plasma is generated by applying a pulsed high-voltage electrical discharge. Previous work reported three-dimensional magnetohydrodynamic simulations

of hydrogen-gas filling and discharge-plasma formation [13]. This approach ionises the gas and creates a plasma channel that acts as a waveguide for the laser pulse. Compared with gas targets ionised solely by the laser pulse, the preformed plasma channel allows the laser to propagate over longer distances within the plasma, overcoming diffraction limitations and enabling the use of laser systems with lower peak power at high repetition rates. Furthermore, these channels improve the efficiency of energy transfer from the laser pulse to the plasma wave, leading to reduced transmission and coupling losses [14]. Hydrogen gas is used to fill the capillary. Under the experimental discharge conditions, a fully ionized hydrogen plasma is produced, which helps minimise both spectral and temporal distortions of the guided laser pulse [15, 16]. Such targets are compatible with high-repetition-rate operation [17] and have been experimentally demonstrated at repetition rates up to the kHz level [18].

Longitudinal plasma density profiles were obtained from time-resolved emission spectroscopy, utilising Stark broadening analysis of the hydrogen Balmer-α (H_α) line at 656.3 nm. Complementary quasi-3D particle-in-cell (PIC) simulations, incorporating experimentally measured longitudinal plasma density profiles, confirm the gas-filled capillary discharge's ability to produce electron beam with mean energy of 670 MeV.

2 Density measurement method

2.1 Experimental setup

The plasma source characterised in this study is a 15 mm-long sapphire capillary with a square cross-section of 300×300 μm, filled with hydrogen. The hydrogen is supplied continuously from an electrolytic generator and introduced into the capillary via two inlets, with the flow regulated by two independent mass flow controllers. The experimental setup is shown in Fig. 1. Plasma is generated by applying a high-voltage electrical discharge with a duration of approximately 300 ns (full width at half

maximum (FWHM)) across two electrodes placed at the ends of the capillary. The discharge can operate at 20 Hz, delivering a peak current of approximately 300 A at an applied voltage of 25 kV. But in this study, the repetition rate was limited to 0.4 Hz by the data acquisition rate of the oscilloscope control software. An example of a discharge-current profile at 25 kV is shown in Fig. 2. The first lens (L_1) collects light emitted from the plasma, which is then focused into a spectrometer (Andor Kymera 328i) using the second lens (L_2). The collected light is dispersed by a diffraction grating with 1200 lines/mm and recorded by an intensified scientific complementary metal-oxide-semiconductor (sCMOS) camera (Andor iStar). An internal delay can be introduced to measure the temporal evolution of the plasma.

For the experiments presented in this paper, we selected the hydrogen H_α line at 656.3 nm because it has a higher transition probability compared to the hydrogen Balmer-β line at 486.1 nm, thereby enhancing the signal-to-noise ratio. The repetition rate was reduced to 0.4 Hz due to the limitation on acquisition speed from the oscilloscope.

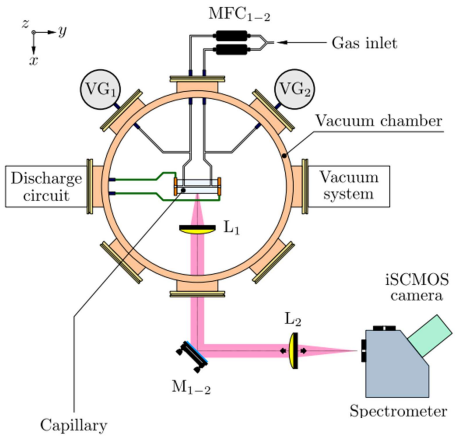


Fig. 1 Schematic diagram of the experimental setup. Labels: MFC- mass flow controller, VG - vacuum gauge, L - lens, M - mirror.

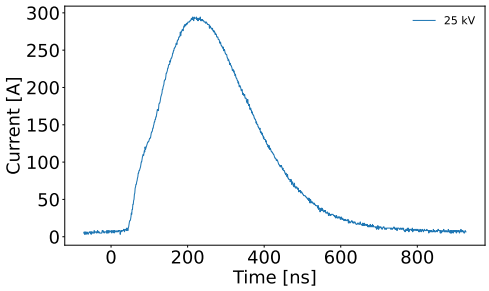


Fig. 2 Discharge-current profile measured at 25 kV for a constant flow of 0.150 mg/s through each gas inlet.

2.2 Stark Broadening method

The application of a high-voltage electrical discharge to the electrodes rapidly increases the electron temperature, driving gas ionisation through collisional processes [16]. This results in a plasma that is either fully or partially ionised, depending on the discharge parameters. The Stark broadening method exploits spectral-line broadening caused primarily by microscopic electric-field fluctuations within the plasma [19]. The plasma electron density n_e is determined from the spectral-line width using the relation [20]:

$$n_e\,[\mathrm{cm}^{-3}] = 8.02 \times 10^{12} \times \left(\frac{\Delta\lambda_{\mathrm{FWHM}}}{\alpha_{H\alpha}}\right)^{3/2}, \tag{1}$$

where $\Delta\lambda_{\mathrm{FWHM}}$ represents the FWHM of the Stark-broadened spectral line in angstroms, and the constant $\alpha_{H\alpha} = 0.0214$ denotes the fractional intensity width of the $H\alpha$ line, derived from electron-temperature and density dependencies [21]. As shown in Eq. (1), broader spectral-line widths measured by the camera correspond directly to higher electron densities. A typical raw image from the sCMOS camera and an example spectral-line profile with its Lorentzian fit are shown in Fig. 3. We extract the fitted $\Delta\lambda_{\mathrm{FWHM}}$ value from each pixel row, enabling reconstruction of the full longitudinal density profile of the capillary.

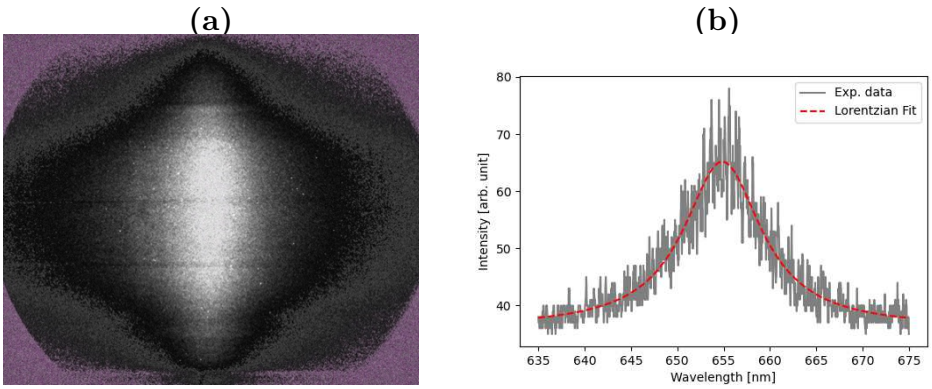


Fig. 3 Stark-broadened spectral-line measurement and fit. (a) Raw spectrometer image. (b) Typical spectral-line profile measured at the capillary centre (grey) with the Lorentzian fitting function (red).

3 Experimental results

Using the experimental setup described in the previous section, we measured the longitudinal electron density profiles by systematically varying both the camera's internal timing delay and the gas flow rate through the inlets. Figures 4(a) and 5(a) show the maximum electron densities measured at flow rates of 0.150 mg/s and 0.075 mg/s per inlet. The peak plasma densities reached 2.4×10^{18} cm^{-3} and 1.3×10^{18} cm^{-3}, respectively. These values are consistent with plasma densities typically used for laser waveguiding in plasma channels, which are generally on the order of 10^{17}–10^{18} cm^{-3}, confirming that the discharge plasma satisfies this condition. However, optimal electron acceleration in LWFA requires operation within the 10^{18} cm^{-3} range, where the wakefield's accelerating gradient scales as $E \propto \sqrt{n_e}$. This density regime is localised between the gas inlets, limiting the effective accelerating region to approximately 60% of the capillary length.

Figure 4(a) exhibits a higher density compared to Fig. 5(a), consistent with the measured total pressures of 85 mbar and 55 mbar, respectively. However, the higher flow regime showed increased instabilities, likely due to incomplete ionisation within the channel. As the discharge current rises, it may remain insufficient to fully ionise

the bulk gas before thermal equilibrium is achieved [14]. We observe in Fig. 4(b) that the maximum density is recorded on the descending slope of the discharge current, 20 ns later, compared to a halved flow rate in Fig. 5(b). The impact of these density fluctuations on LWFA performance is investigated via quasi-3D PIC simulations in the following section.

Moreover, by adjusting the delay on the camera, we performed a temporal evolution scan of plasma formation at a flow rate of 0.075 mg/s per inlet, and the results are presented in Fig. 6(a). In Fig. 6(b), we present the discharge current, with the coloured hashed section representing the time frame during which the camera acquires the signal for 10 ns. This analysis also highlights the importance of controlling laser-target synchronisation with a jitter of less than 80 ns. Results demonstrate that a laser arrival on target within $\leq$ 80 ns at the peak plasma density will result in minimal density variation. However, beyond this threshold, the density decreases by approximately 30% of the peak value.

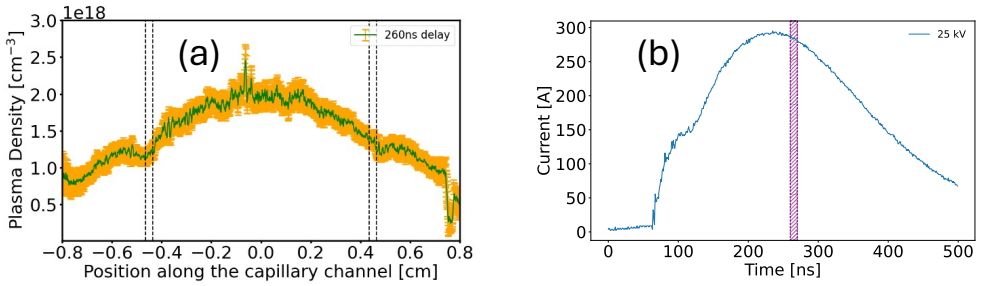


Fig. 4 Plasma density and discharge current at 0.150 mg/s. (a) Longitudinal plasma-density profile averaged over 50 images. Dashed black regions indicate gas-inlet positions. The top-right value denotes the camera-acquisition delay (10 ns resolution) relative to discharge triggering. (b) Discharge current profile at 25 kV. The coloured hatched region represents the camera-acquisition window.

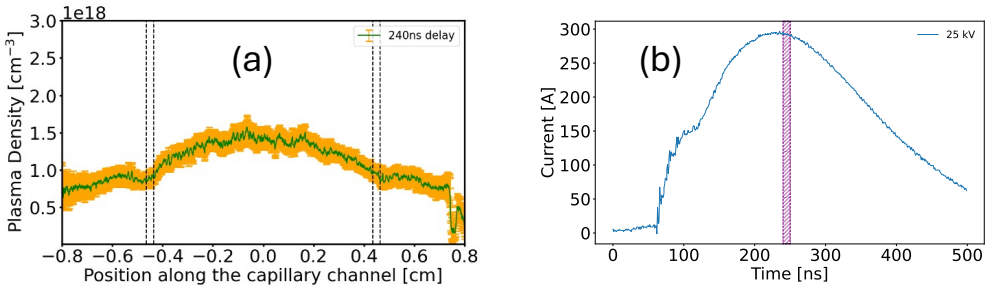


Fig. 5 Plasma density and discharge current at 0.075 mg/s. (a) Longitudinal plasma-density profile averaged over 50 images. Dashed black regions indicate gas-inlet positions. The top-right value denotes the camera-acquisition delay (10 ns resolution) relative to discharge triggering. (b) Discharge-current profile at 25 kV. The coloured hatched region represents the camera-acquisition window.

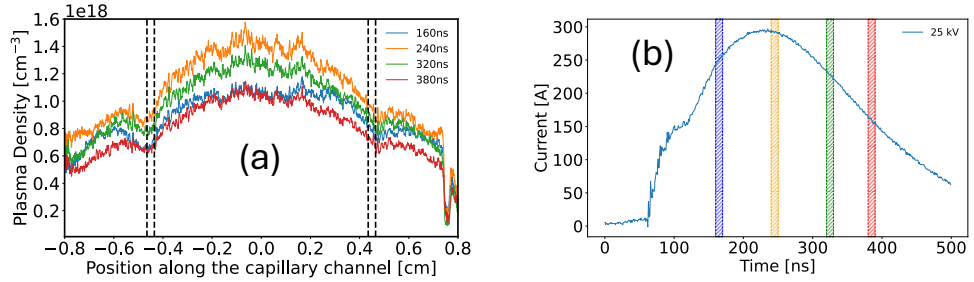


Fig. 6 Temporal evolution of the discharge plasma. (a) Longitudinal plasma-density profiles averaged over 50 images for a gas-inlet flow of 0.075 mg/s. Dashed black regions indicate gas-inlet positions. The top-right values denote camera-acquisition delays (10 ns resolution) relative to discharge triggering. (b) Discharge-current profile at 25 kV. The coloured hatched regions show the camera-acquisition window for each delay in panel (a).

4 Particle-in-cell simulations

4.1 Laser guiding structure

During plasma formation, the transverse electron density is higher near the capillary walls than on axis, producing a parabolic plasma channel. The associated radial variation in density modifies the plasma refractive index and enables laser guiding along the capillary axis. In the transverse direction, the electron density profile can be approximated by a parabolic form [16]:

$$n_e(r) \approx n_e(0)\left(1 + 0.33\frac{r^2}{R_{\mathrm{cap}}^2}\right), \tag{2}$$

where R_{cap} is the capillary radius, equal in this work to 150 μm.

A parabolic channel alone is not sufficient to ensure guiding; the laser spot must be properly matched to the plasma channel so that the refractive-index gradient can confine the beam. If the matching condition is not satisfied, the laser will instead undergo self-focusing within the plasma. The matched spot radius is given by [16]:

$$w_m\,[\mu\mathrm{m}] \approx \frac{1.45\times10^5}{2}\frac{\sqrt{R_{\mathrm{cap}}\,[\mu\mathrm{m}]}}{\left(n_e\,[\mathrm{cm}^{-3}]\right)^{1/4}}, \tag{3}$$

where w_m denotes the matched laser waist.

4.2 Simulation results

Particle-in-cell (PIC) simulations were carried out with the SMILEI code [22] in a quasi-3D geometry assuming azimuthal symmetry. The azimuthal degree was 2 and a macroparticle configuration of (2×1×8) particles per cell was used along the (x, r, θ) directions, respectively, corresponding to a total of 16 macroparticles per cell. The computational domain employed a moving window propagating at the speed of light, with a transverse (radial) extent of 154λ resolved with a grid spacing of $\lambda/2.5$, and a longitudinal length of 102λ resolved with a grid spacing of $\lambda/50$; the time step was set to $\lambda/(51c)$, where λ is the laser wavelength and c is the speed of light in vacuum. The driving laser pulse was modelled as a linearly polarized Gaussian beam propagating along the x axis with polarization along the y axis. The laser parameters used in the simulations are based on those of the L2-DUHA laser [10], which will drive the LUIS beamline [11] at the ELI ERIC facility. The laser has a central wavelength of 820 nm, a pulse energy of 2 J, and a pulse duration of 30 fs (FWHM). The experimentally measured longitudinal plasma density profile, shown in Fig. 4(a), was used in the simulations, while the transverse density distribution was prescribed by Eq. (2). The simulation results are presented in Figs. 7 and 8. Figure 7 shows the on-axis plasma-density profile extracted from the PIC simulations together with the evolution of the

normalised vector potential a_0 as a function of laser-propagation distance. Two laser spot sizes, $w_0 = 20$ μm and 30 μm, were studied at the same laser energy, with a_0 adjusted according to the beam waist. For $w_0 = 20$ μm, the laser was initially focused at $x = 4.0$ mm and underwent self-focusing during propagation. Consequently, a_0 increased beyond its vacuum-focus value of about 2.3, reached a peak above 3.7, and then decreased through the plasma-density profile. In contrast, for $w_0 = 30$ μm with an initial focus at $x = 4.0$ mm, a_0 rose above its vacuum-focus value of about 1.5 and then remained nearly constant across the density plateau, indicating effective laser guiding. For the present plasma density, Eq. (3) gives a matched radius of approximately 26 μm, consistent with guiding for the larger spot size and self-focusing for the smaller one.

In practice, the laser spot size is typically constrained by the focusing optic upstream of the target. Although the capillary radius R_{cap} could be reduced, this would approach manufacturing limits and impose tighter requirements on laser pointing stability. Alternatively, the plasma density can be increased to achieve a larger matched laser spot size; for the present capillary geometry and $w_0 = 20$ μm, the required density would be approximately 4×10^{18} cm^{-3}, which could be obtained experimentally by raising the gas pressure inside the capillary, and increasing accordingly the high-voltage discharge.

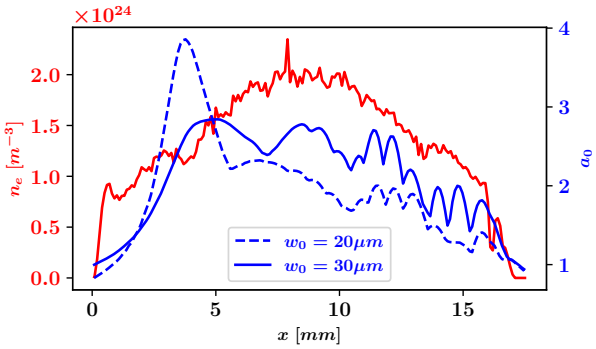


Fig. 7 Laser evolution in the discharge-plasma channel. On-axis plasma density n_e (red) and peak normalised vector potential a_0 as functions of laser-propagation distance for laser waists w_0 of 20 μm (dashed blue line) and 30 μm (solid blue line).

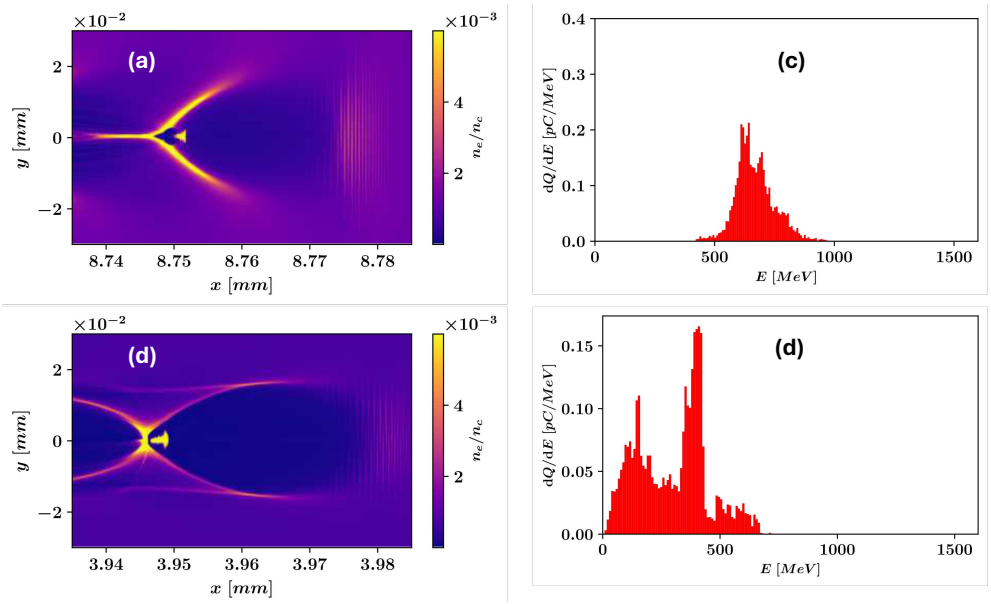


Fig. 8 Electron injection and energy spectra. Plasma electron density in the x-y plane showing the injected electrons in the first wake structure behind the laser pulse for (a) $w_0 = 30$ μm and (b) $w_0 = 20$ μm. Electron-beam energy spectra at the plasma exit ($x = 17.5$ mm) for (c) the guided laser beam with $w_0 = 30$ μm and (d) the self-focusing laser beam with $w_0 = 20$ μm.

In both cases, electrons are injected and trapped in the first plasma bubble behind the laser pulse through self-injection, as shown in Fig. 8. The results for $w_0 = 30$ μm and $w_0 = 20$ μm are presented in Fig. 8(a) and (b), respectively. In the guided case, Fig. 8(c) shows that a 15 mm-long discharge capillary driven by a 2.0 J guided laser pulse can produce electron beams with a charge of 30 pC, a mean energy of 670 MeV, and an RMS energy spread of approximately 20%. The beam has an RMS divergence of about 1.2 mrad horizontally and 1.1 mrad vertically, with corresponding RMS normalised emittances of 1.18 mm·mrad and 1.01 mm·mrad, respectively. By contrast, the non-guided case in Fig. 8(d) yields substantially poorer beam quality, with a charge of 32 pC, a mean energy of 302 MeV, and an RMS energy spread over 100%. The corresponding RMS divergence increases to 11.9 mrad horizontally and 15.3 mrad vertically, with normalised emittances of 2.08 mm·mrad and 2.74 mm·mrad, respectively. These results highlight the importance of operation in the guided regime,

since the longitudinal plasma-density profile created by electrical discharge is otherwise insufficiently homogeneous to support the production of high-quality electron beams.

5 Conclusion and perspectives

We have presented the characterisation of the longitudinal plasma density profile for a 15 mm long sapphire capillary, achieving a peak density of 2.4×10^{18} cm^{-3} under the discharge conditions of 25 kV and 0.150 mg/s per gas inlet. The results reveal a stable high-density region over 10^{18} cm^{-3} covering 60% of the capillary length. This finding motivates further studies with extended capillaries to fully exploit the accelerating potential over longer interaction lengths. In parallel, future developments will focus on increasing the discharge repetition rate through the implementation of a new power supply capable of higher repetition rate operation.

Quasi-3D PIC simulations, incorporating the experimentally measured longitudinal plasma density profile and laser parameters representative of the high-repetition-rate L2-DUHA laser system, demonstrated effective electron beam acceleration along the plasma channel. In the guided regime, the electron beam reached a mean energy of approximately 670 MeV while maintaining reasonably good transverse properties. However, the energy spread remains relatively high and will require further optimisation for future application as an FEL driver.

By contrast, in the non-guided regime, the electron beam exhibits poorer beam quality but higher charge, which may be advantageous for applications beyond light sources, such as medical uses. However, by optimising the capillary geometry and tuning the gas parameters, the resulting plasma density profile can be improved, which may enhance the beam quality in both configurations. For example, our recent study, based on a combination of hydrodynamic and PIC modeling, proposed a specially designed capillary setup to generate GeV-class, high-quality electron beams via LWFA, which could be compatible with the development of LWFA-based FELs in the EUV

regime [23]. A detailed experimental investigation of such capillary setups will be pursued in future studies.

List of abbreviations

EUV, extreme ultraviolet; FEL, free-electron laser; FWHM, full width at half maximum; LPA, laser-plasma accelerator; LWFA, laser wakefield acceleration; PBA, plasma-based accelerator; PIC, particle-in-cell; PWFA, plasma wakefield acceleration; RMS, root mean square; sCMOS, scientific complementary metal-oxide-semiconductor.

Declarations

Availability of data and materials

The datasets used and analysed during the current study are available from the corresponding author on reasonable request.

Competing interests

The authors declare that they have no competing interests.

Funding

This work was supported by the European Union's Horizon Europe research and innovation programme under grant agreement no. 101079773 (EuPRAXIA Preparatory Phase), no. 101188004 (PACRI–Plasma Accelerator systems for Compact Research Infrastructures), and no. 101073480 and the UKRI guarantee funds (EuPRAXIA Doctoral Network), and by the Ministry of Education, Youth and Sports of the Czech Republic through the e-INFRA CZ, ID:90254.

Authors' contributions

AW conducted the experimental data analysis, lead the manuscript preparation. AW, MiM, AM conceptualised the work. AW, MiM, SM, and MaM contributed to the simulations and analysis of the data. AW, MiM, AJ prepared the experimental setup and acquired the experimental data. PVS provided theoritical support. SN and PZ prepared the control system. AJ, JTG and AM supervised the project. All authors reviewed the manuscript and approved the final version.

Acknowledgements

Not applicable.

Ethics approval and consent to participate

Not applicable.

Consent for publication

All authors approved the manuscript and consent to its publication.

References

[1] Tajima T, Dawson JM. Laser electron accelerator. Phys Rev Lett. 1979;43:267–270. https://doi.org/10.1103/PhysRevLett.43.267.

[2] Chen P, Dawson JM, Huff RW, Katsouleas T. Acceleration of electrons by the interaction of a bunched electron beam with a plasma. Phys Rev Lett. 1985;54:693–696. https://doi.org/10.1103/PhysRevLett.54.693.

[3] Bohlen S, Wood JC, Brümmer T, et al. Stability of ionization-injection-based laser-plasma accelerators. Phys Rev Accel Beams. 2022;25:031301. https://doi.org/10.1103/PhysRevAccelBeams.25.031301.

[4] Wang WT, Li WT, Liu JS, et al. High-Brightness High-Energy Electron Beams from a Laser Wakefield Accelerator via Energy Chirp Control. Phys Rev Lett. 2016;117:124801. https://doi.org/10.1103/PhysRevLett.117.124801.

[5] Wang W, Feng K, Ke L, et al. Free-electron lasing at 27 nanometres based on a laser wakefield accelerator. Nature. 2021;595:516–520. https://doi.org/10.1038/s41586-021-03678-x.

[6] Pompili R, Alesini D, Anania MP, et al. Free-electron lasing with compact beam-driven plasma wakefield accelerator. Nature. 2022;605:659–662. https://doi.org/10.1038/s41586-022-04589-1.

[7] Labat M, Cabadağ JC, Ghaith A, Irman A, Berlioux A, Berteaud P, et al. Seeded free-electron laser driven by a compact laser plasma accelerator. Nature Photonics. 2023;17(2):150–156.

[8] Barber SK, Kohrell F, Doss CE, Jensen K, Berger C, Isono F, et al. Greater than 1000-fold Gain in a Free-Electron Laser Driven by a Laser-Plasma Accelerator with High Reliability. Phys Rev Lett. 2025 Jul;135:055001. https://doi.org/10.1103/vh62-gz1p.

[9] Kohrell F, Barber SK, Doss CE, Jensen K, Schröder S, Berger C, et al. Over 8 hours of continuous operation of a free-electron laser driven by a laser-plasma accelerator. Phys Rev Accel Beams. 2026 Apr;29:041301. https://doi.org/10.1103/z2d3-bhyt.

[10] Green JT, Antipenkov R, Bakule P, et al. L2-DUHA 100 TW high repetition rate laser system at ELI-Beamlines. Key design considerations. Rev Laser Eng. 2021;49:106–109. https://doi.org/10.2184/lsj.49.2_106.

[11] Molodozhentsev AY, Kruchinin KO. Compact LWFA-based extreme ultraviolet free electron laser: Design constraints. Instruments. 2022;6(1):4.

[12] Assmann R, Weikum M, Akhter T, Alesini D, Alexandrova A, Anania M, et al. EuPRAXIA conceptual design report. The European Physical Journal Special Topics. 2020;229(24):3675–4284.

[13] Bagdasarov GA, Kruchinin KO, Molodozhentsev AY, Sasorov PV, Bulanov SV, Gasilov VA. Discharge plasma formation in square capillary with gas supply channels. Phys Rev Research. 2022;4:013063. https://doi.org/10.1103/PhysRevResearch.4.013063.

[14] Kruchinin KO, Mondal A, Sasorov PV, Zimmermann P, Niekrasz S, Molodozhentsev AY. Experimental characterization of discharge plasma dynamics in a square capillary for prospective applications in laser wakefield acceleration. Phys Plasmas. 2025;32:043511. https://doi.org/10.1063/5.0260100.

[15] Nakamura K, Nagler B, Toth C, et al. GeV electron beams from a centimeter-scale channel guided laser wakefield accelerator. Phys Plasmas. 2007;14:056708. https://doi.org/10.1063/1.2718524.

[16] Bobrova NA, Esaulov AA, Sakai JI, Sasorov PV, Spence DJ, Butler A, et al. Simulations of a hydrogen-filled capillary discharge waveguide. Phys Rev E. 2001;65:016407. https://doi.org/10.1103/PhysRevE.65.016407.

[17] Sasorov P, Bagdasarov G, Bobrova N, Grittani G, Molodozhentsev A, Bulanov S. Capillary discharge in the high repetition rate regime. Physical Review Research. 2024;6(1):013290.

[18] Gonsalves A, Liu F, Bobrova N, Sasorov P, Pieronek C, Daniels J, et al. Demonstration of a high repetition rate capillary discharge waveguide. Journal of Applied

Physics. 2016;119(3).

[19] Sobelman II. Atomic Spectra and Radiative Transitions. Berlin: Springer-Verlag; 1992.

[20] Jang DG, Kim MS, Nam IH, Uhm HS, Suk H. Density evolution measurement of hydrogen plasma in capillary discharge by spectroscopy and interferometry methods. Appl Phys Lett. 2011;99. https://doi.org/10.1063/1.3643134.

[21] Griem HR. Spectral Line Broadening by Plasmas. New York: Academic Press; 1974.

[22] Derouillat J, Beck A, Pérez F, Vinci T, Chiaramello M, Grassi A, et al. Smilei: a collaborative, open-source, multi-purpose particle-in-cell code for plasma simulation. Comput Phys Commun. 2018;222:351–373. https://doi.org/10.1016/j.cpc.2017.09.024.

[23] Maity S, Massimo F, Whitehead A, Sasorov P, Molodozhentsev A. Laser wakefield acceleration in a capillary gas cell to produce high-quality GeV-scale electron beams. Phys Rev Accel Beams. 2026 Aug;https://doi.org/10.1103/l8b2-j67x.